Estimation of past atmospheric carbon dioxide levels using tree-ring cellulose $\delta^{13}C$

Trina Bose[1,*], Supriyo Chakraborty[1], Hemant Borgaonkar[1], Saikat Sengupta[1] and R. Ramesh[2]

[1]Indian Institute of Tropical Meteorology, Pune 411 008, India
[2]Physical Research Laboratory, Ahmedabad 380 009, India

We study the applicability of the Farquhar model for carbon isotopic discrimination (change in carbon isotopic composition from air CO_2 to tree-ring cellulose) in C_3 plants to trees growing in the field. Two new carbon isotope datasets from Himalayan conifers with published data from another eight sites across the world show disparate trends in the plot of carbon isotope discrimination versus atmospheric carbon dioxide concentration, in contrast to the model prediction of absence of any trend. This is because the model assumes that the tree adjusts its stomatal conductance for water-use efficiency to maintain a constant ratio of carbon dioxide concentrations inside and outside the leaf and treats the diffusive and biochemical fractionation factors as constants. By introducing a simple linear dependence of these fractionation factors with ambient temperature and humidity, we have enhanced the applicability of the model to naturally growing trees. Further, despite the disparate trends exhibited by the 10 trees, we show using the inverse modelling that it is possible to derive a unique record of past atmospheric CO_2 concentrations using tree cellulose $\delta^{13}C$ data. The reconstructions also replicate the summer pCO_2 gradient from tropics to mid-latitudes. We also discuss the merits and demerits of the model, and compare the model-derived pCO_2 with that of the ice core-based records from Law Dome.

Keywords: Atmospheric carbon dioxide, carbon isotope, cellulose, climate change, tree ring.

THE recent progressive increase of the atmospheric carbon dioxide concentration (c_a) has earned considerable attention due to its role in global climate change. This has necessitated the identification of sources and sinks of this atmospheric gas. Although a few sources and sinks have been identified from the instrumental data[1], such studies are limited due to short-time range of the dataset. The only long-term (1800–1978 CE) annual c_a data that can be validated against instrumental observations are available from ice cores of Law Dome, Antarctica[2]. The preceeding ice core data with resolution of 2–10 years stop at 1939 (ref. 3). There are some pCO_2 data from the Greenland ice cores which reach mid-1900s (ref. 4), but they have very low resolution for comparison in annual scale. The Law Dome ice core data[2] is used in this study for comparison because it provides better resolution and maximum overlapping period with instrumental datasets relative to other ice-core records.

In view of the modern pCO_2 distribution and fluxes (Rödenbeck *et al.*[1] and references therein), it is apparent that the latitudinal distribution of pCO_2 and the difference in various fluxes between the continents cannot be studied using the ice-core data alone. This is because there are no reconstructed CO_2 datasets representing the tropics and sub-tropics before 1950s. The paucity of high-resolution data in space and time limits the application of ice-core CO_2 data for studying the past carbon fluxes[1].

One of the main sinks of atmospheric CO_2 are the trees that comprise ~95% of land biomass[5]. The long-living (up to a few millennia) trees fix carbon in ring cellulose, and are datable to annual to sub-annual resolution[6,7]. So stable carbon isotope ratios of cellulose ($\delta^{13}C_c$) may be an independent alternative for the determination of c_a. This has been hampered by the dependence of $\delta^{13}C_c$ on multiple environmental and tree-specific parameters[8]. Carbon isotope records of tree rings have been successfully used for a variety of palaeoclimate and environmental studies[9–17] including their relationship with pCO_2, temperature and humidity[18,19]. However, these studies stop short of reconstructing c_a time series from $\delta^{13}C_c$ of trees growing in natural environments.

Carbon isotope fractionation in trees grown in controlled environments was investigated in detail by Farquhar *et al.*[20] in the early 1980s, who formulated a model for calculating the carbon isotope discrimination (d) in terms of biophysical parameters of the tree and its surroundings, such as pCO_2 and $\delta^{13}C$ of air (c_a and $\delta^{13}C_a$) and intercellular CO_2 (c_i) in plant materials. The model suggests that c_a is not proportional to d due to the plants adjusting stomatal conductance/density to optimize water-use efficiency so as to maintain a constant ratio of pCO_2 in intercellular spaces relative to atmosphere (c_i/c_a). Their model, however, does not address possible effects of a sharp rise in atmospheric pCO_2 as seen in last few decades, on d.

The effect of rising pCO_2 was shown experimentally by Evans and Von Caemmerer[21]. They showed that diffusion

*For correspondence. (e-mail: trina@tropmet.res.in)

of CO_2 from the atmosphere to the confines of the leaf may be considered as that from an infinite reservoir to a finite one. Hence, while c_i should be linearly proportional to initial values of c_a, it would saturate at higher values of c_a, when other factors remain constant[21]. Hence, the plot of c_i/c_a versus c_a should initially remain constant and then fall rapidly with c_a. By this consideration, the c_i/c_a versus c_a (or d versus c_a) plot should show a negative slope at higher values of c_a.

Here, we examine whether the said relationship holds true for naturally growing trees as well. For this, we consider pre-industrial $\delta^{13}C_a$ to be constant and decreasing continuously since the advent of the industrial revolution[22], as a result of fossil-fuel emission. The relationships between d and other meteorological parameters are also studied in this context. Our study shows that Farquhar model does not apply to all cases of natural trees. We further demonstrate that inclusion of variability of meteorological parameters also improves the applicability of the Farquhar model. The modified model is calibrated for the period 1978–2005 CE and tested for congruency with observations during 1958–1977 CE (testing period). Finally, c_a has been reconstructed for the period 1902–1957 CE, and compared with Law Dome ice core pCO_2 data. This reconstruction fills the pCO_2 data gap in the sub-tropics and tropics from 1958 to 1901. Till now, there were no means to study the summer pCO_2 gradient between the tropics and the mid latitudes, which is reproduced using our reconstruction.

Data choice and testing

To apply the model of Farquhar *et al.*[20] to trees from natural settings, we calculated the slope of d versus c_a plot using $\delta^{13}C_c$ data of such trees. Additionally, we needed to study the effects of meteorological parameters on $\delta^{13}C_c$. Such data collected from various sources mentioned below.

Tree ring cellulose $\delta^{13}C$

Two of the testing datasets (carbon isotopes) were generated in the present study. These samples were collected from the Western Himalayas; (i) Kanasar, Uttarakhand, India (*Cedrus deodara*), (ii) Kothi, Himachal Pradesh, India (*Picea smithiana*) and dated by dendrochronological methods[23,24] before isotopic analysis. The wider rings were separated manually using hammer and chisel, while the thinner rings were separated using a sledge microtome (Fritz Hans Schweingruber, Switzerland)[25]. Cellulose extraction was carried out following Leavitt–Danzer method[7], with minor modifications. The samples were analysed at the Stable Isotope Laboratory, IITM, India using a Delta-V Plus isotope ratio mass spectrometer (Thermo Fisher Scientific) equipped with a Flash EA 1112 Elemental Analyser in continuous flow mode. IAEA primary reference materials [CH3: $\delta^{13}C = -24.724$‰ VPDB and CH6: $\delta^{13}C = -10.449$‰ VPDB] were used for calibration. Standard deviation of the IAEA CH3 was ± 0.02‰ and that of IAEA-CH6 was ± 0.08‰. The routine precision based on sample replicates of our measurement was ± 0.1‰. All values are reported against VPDB scale and presented in Figure 1. The black and grey curves show $\delta^{13}C$ variations of *C. deodara* and *P. smithiana* respectively.

Additionally, we have used tree-ring $\delta^{13}C_c$ data from eight stations across the globe[12–17]. Sample sets with site locations, code names and lengths of these records are shown in Figure 2 (see also Table 1).

Atmospheric carbon dioxide data

Atmospheric pCO_2 (1957–2008 CE) and $\delta^{13}C$ of atmospheric CO_2 (1977–2008 CE) data from 11 Scripps Institution of Oceanography (SIO) stations were used in the present study[26]. For testing the latitudinal gradient we have also used CO_2 data from Cape Fergusson, Australia (http://cdiac.ornl.gov/trends/co2/csiro/csiro-cferg.html). The Australian site was chosen because the SIO sites at similar latitudes were island sites.

The annual average c_a for all sites shows very low spatial variability (<2 ppm maximum standard deviation, i.e. maximum of spatial standard deviation among all 11 site annual averages and all years). However, the annual minimum (corresponding to maximum photosynthesis by plants) and maximum (indicating maximum decomposition/plant respiration) values are characterized by higher spatial variability (<4 ppm). The maximum monthly spatial

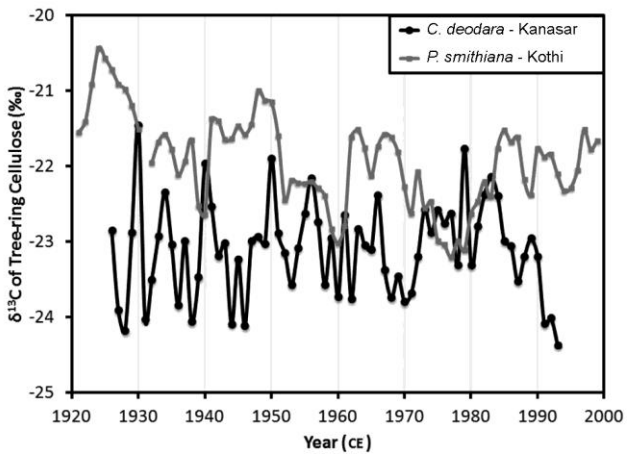

Figure 1. $\delta^{13}C_c$ records of *Cedrus deodara* (black line) from Kanasar, Uttarakhand (77°48′, 30°45′, 2200 m amsl) and *Picea smithiana* (grey line), from Kothi, Himachal Pradesh (77°17′, 32°25′; 2500 m amsl) in the Western Himalayas. As these stations are ~200 km apart in different drainage and climatic settings, they are not expected to have much coherence in $\delta^{13}C_c$. Annual rings of *C. deodara* were separately analysed in early wood and late wood samples and an average $\delta^{13}C_c$ was taken for this study. Annual rings were analysed for *P. smithiana*.

Table 1. For all sites, chosen values of h for the reconstruction are shown with the corresponding P_r (average absolute difference between observed global annual average c_a and model output c_a) and $mxr\sigma$ (maximum reconstruction error between all time steps). The h values of similar species do not differ significantly even with large geographical separation, e.g. the *Picea* from India (KOHP) and Siberia (MRUS) show similar h values. Samples from nearby sites with different genera, e.g. CASW and VISW show different h values

Site code	Longitude (°)	Latitude (°)	Altitude (m amsl)	Species	Reference	Data range (CE)	h (‰/ppm)	P_r (ppm)	$mxr\sigma$ (ppm)
PMPE	–69	–13	265	*Cedrela odorata*	16	1820–2004	0.31	1.16	1.16
BWCA	–118	37	3200	*Pinus longaeva*	17	1085–2005	0.46	0.91	0.99
MRUS	60	68	40	*Picea obovata*	12	1905–1996	0.42	0.78	0.56
LOSW	8	46	2000	*Larix decidua*	15	1650–2004	0.35	1.18	1.47
CASW	9	46	900	*Quercus petraea*	13	1637–2002	0.38	0.76	0.79
VISW	8	48	1400	*Pinus sylvestris*	13	1675–2003	0.27	1.29	1.33
BAGR	75	36	2900	*Juniperus excelsa*	14	1900–1998	0.24	0.58	0.59
BOIB	75	37	3900	*Juniperus turkestanica*	14	1950–1998	0.3	0.71	0.71
KAUT	78	31	2200	*Cedrus deodara*	Present work	1925–1993	0.64	1.45	0.60
KOHP	77	32	2500	*Picea smithiana*	Present work	1920–1999	0.45	1.16	0.79

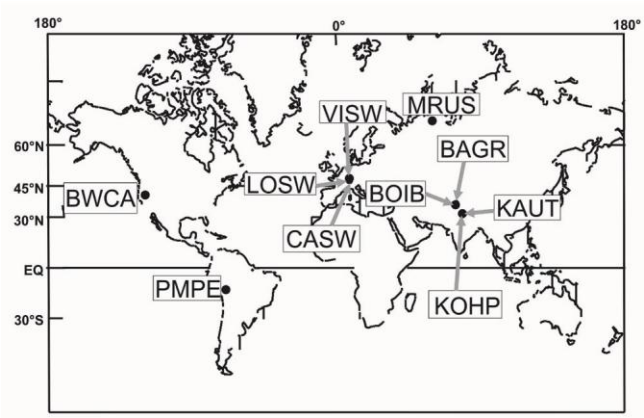

Figure 2. Location map of the ten tree-ring sites whose $\delta^{13}C_c$ records have been used in this study. Table 1 provides information on site name, longitude, latitude, altitude, name of the species and duration of $\delta^{13}C_c$ time series for all sites.

variability of c_a among the stations is ~4.1 ppm, which possibly corresponds to local differences in peak productivity periods.

Like c_a, $\delta^{13}C_a$ also shows very low spatial variability in the annual average (<0.11‰). But the monthly spatial variability maximum for $\delta^{13}C_a$ is 0.23‰. The maximum range in any of the SIO stations is at Point Barrow, Alaska (for all years: average 0.87‰, maximum 0.98‰, minimum 0.74‰) followed by Alert, NWT, Canada (for all years: average 0.79‰, maximum 0.94‰, minimum 0.69‰). The lowest range is seen in American Samoa (for all years: average 0.08‰, maximum 0.16‰, minimum 0.04‰) followed by South Pole (for all years: average 0.79‰, maximum 0.94‰, minimum 0.69‰) and Kermadec Islands (for all years: average 0.79%, maximum 0.94‰, minimum 0.69‰). This range represents the fact that in the productive period (c_a minimum), trees show a preference towards ^{12}C, thus leaving air enriched in ^{13}C; this extra ^{12}C is released back in air during decomposition making atmospheric CO_2 isotopically lighter[27]. Further, Levin *et al.*[28] after analysing multiple sites in Germany showed that this range can vary even among nearby places and depends on altitude or nearby plant concentration.

For input to the model for the time period 1901–2005 CE, a quadratic fit (the linear correlation coefficient, $r = 0.99$) of the instrumental $\delta^{13}C_a$ (global annual average) with time (years) was used to extend the $\delta^{13}C_a$ values back in time with maximum value set at the pre-industrial value of –6.4‰ (ref. 22). Global annual average of $\delta^{13}C_a$ was used because of non-availability of $\delta^{13}C_a$ data for most tree-ring sites (nearest available $\delta^{13}C_a$ data are ~500 km from BWCA) and no clear pattern of $\delta^{13}C_a$ annual range depending on latitude.

d versus c_a slope estimation and analysis

As instrumentally observed $\delta^{13}C_a$ data is only available after 1977 CE, the d and c_a relationship is studied for 1978–2005 CE using the observed values. Figure 3 (details in Table 2) shows that at two locations, d and c_a have no significant correlation ($r = -0.12$ for KOHP to 0.26 for BWCA with $P > 0.19$). The remaining eight locations show positive trends ($r = 0.53$ to 0.93; $P < 0.02$). Similar positive slopes were also reported for plants grown under controlled environment[19]. These trends are a serious departure from the model of Farquhar *et al.*[20]. The observed positive trend cannot be explained by the model unless we consider the two fractionation factors a (for diffusion) and b (for carboxylation) to be controlled by meteorological parameters, such as temperature and humidity.

Meteorological data

To test the effect of meteorological parameters on a and b, we use the Climate Research Unit (CRU) datasets[29] as: (i) they have the highest resolution; (ii) they are derived mostly from observations that represent the complex site topography better; (iii) they are available at all the site

Table 2. Results of statistical analysis for relationship between d and c_a. Highly positive slopes have high and significant r and stations with low slope values (+/–) show low r. The r values do not show any dependence on geographical location or nearness to industrial regions

	PMPE	BWCA	MRUS	LOSW	CASW	VISW	BAGR	BOIB	KAUT	KOHP
Number of points	27	27	19	27	25	26	21	21	16	21
Degrees of freedom	25	25	17	25	23	24	19	19	14	19
Residual sum of squares	1.73	2.07	8.40	7.23	7.21	2.98	2.00	1.42	4.11	2.84
R (%)	70.01	25.93	52.82	75.65	78.63	86.32	82.76	92.52	74.14	11.79
R significance (%)	100.00	80.85	97.99	100.00	100.00	100.00	100.00	100.00	99.90	38.91
Intercept										
Value	11.33	8.58	–4.03	–1.06	–5.95	–1.85	–6.86	–13.85	–15.54	17.78
Error	1.46	1.60	7.02	2.98	3.54	2.08	2.74	2.31	6.95	3.26
t-value	7.77	5.38	0.57	0.35	1.68	0.89	2.51	6.00	2.23	5.46
Probability of intercept, p_i (<)	0.00	0.00	0.60	0.75	0.02	0.40	0.03	0.00	0.05	0.00
Slope										
Value	0.02	0.01	0.06	0.05	0.06	0.05	0.05	0.07	0.09	–0.01
Error	0.41	0.45	2.01	0.84	1.00	0.59	0.78	0.66	2.00	0.93
t-value	5.10	1.70	2.82	5.98	6.31	8.61	6.67	10.95	4.39	1.13
Probability of slope, p_s (<)	0.00	0.02	0.02	0.00	0.00	0.00	0.00	0.00	0.00	0.30

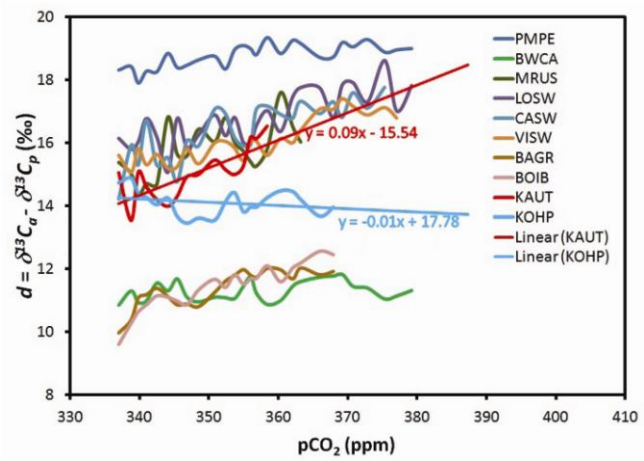

Figure 3. d versus c_a plot for all the stations showing the trend and range of variability. The trends of the two sites, KAUT and KOHP, India have been calculated and plotted as red and cyan lines respectively. It can be noted that in most cases the trend lines are positive in contrast to the expected values from the Farquhar model; only BWCA and KOHP (no trend) results are consistent with the model prediction.

locations relatively for longer time duration (1901–2008 CE) compared to other datasets. Vapour pressure rather than precipitation is taken as representative of the moisture here. This is because evapotranspiration from leaves rather than the amount of soil moisture decides the stomatal opening[30], which in turn decides the rate of diffusion of CO_2 into the leaf.

The modified model

Modifications

Isotopic fractionation during carbon fixation is mainly governed by two processes: (i) gaseous diffusion through stomata of leaves; (ii) the chemical process of carboxylation and deposition. Considering these fractionation pathways, Farquhar *et al.*[20] suggested that net ^{13}C change from air to cellulose (d) can be estimated as

$$d = \delta^{13}\mathrm{C_a} - \delta^{13}\mathrm{C_c} = a + (b-a)\frac{c_\mathrm{i}}{c_\mathrm{a}} - B\frac{c_\mathrm{i}-c_\mathrm{c}}{c_\mathrm{a}}, \quad (1)$$

where a, b and B are fractionation due to diffusion of CO_2 from air to leaves, carboxylation in the leaves forming sugar, and transport of CO_2 from intercellular spaces of leaves to the carboxylation respectively. c_i and c_c are partial pressure of CO_2 in the intercellular spaces of leaves and in the site of carboxylation. It is to be noted that Farquhar *et al.*[20] treated b and B as equal and same, but we have written them as different for process-based differentiation.

We propose the following modifications to apply the model of Farquhar *et al.*[20] for trees growing in the field.

1. The variables c_c and c_i are not measurable in these cases and need to be estimated by some alternative means.
   (i) c_c is about 30% lower than c_i for many species when leaves are actively photosynthesizing in high irradiance[21]. However, this value of 30% will not be applicable to low irradiance zones. Let c_c to be about x% lower than c_i for all cases. Hence $c_\mathrm{c} \approx (1 - \frac{x}{100})\, c_\mathrm{i}$ or

$$\frac{c_\mathrm{i}-c_\mathrm{c}}{c_\mathrm{a}} \approx \frac{x}{100}\frac{c_\mathrm{i}}{c_\mathrm{a}}.$$

So, eq. (1) can be modified as

$$d = a + \left(b - a - \frac{x}{100}B\right)\frac{c_\mathrm{i}}{c_\mathrm{a}}. \quad (2)$$

Now if we define b^* as the fractionation due to the total chemical process, i.e. $b^* = b - \frac{x}{100}B$ we get

$$d = a + (b^* - a)\frac{c_i}{c_a}. \quad (3)$$

(ii) Since c_i is unknown for natural sites, this term is eliminated by considering c_i/c_a as a simple sigmoidal function of c_a, following Evans and Von Caemmerer[21]. This particular function was chosen because it mimics the required variation almost exactly and has a one-to-one correspondence with c_a. As the pCO_2 concentration in water controls pH values in most natural water bodies through carbonate and bicarbonate ions[31], c_i should also be taken as a proxy for the pH of leaf water in the long term (i.e. annual).

$$\frac{c_i}{c_a} = \frac{\gamma}{1 + e^{((sl - c_a)/100)}} = \gamma z, \quad (4)$$

where sl is the level of c_a at which diffusion saturates and γ is the constant of proportionality between c_i/c_a and z.

2. As discussed above, the reason for some stations showing positive instead of no slope predicted by Farquhar *et al.*[20], is perhaps that a and b^* are not constant but vary with meteorological parameters. Temperature and relative humidity dependence of leaf $\delta^{13}C$ was studied in the controlled condition by Edwards *et al.*[32]. Based on this premise, we attempt to modify these factors (a and b^*) as:

(i) Diffusion as a physical process should be dependent on temperature (thermal energy provides kinetic energy which translates into velocity) and moisture content of air (which decides the aperture of the stomata). Diffusion is defined as random movement with resultant directional displacement (mean free path), which is governed by the cross-sectional area, thermal energy and concentration gradient. The diffusion coefficient for gases is inversely proportional to square root of the molecular mass and directly proportional to the cube of square root of temperature[33]. Further, this movement is integrated over the minimum cross-sectional area in the path. So theoretically, there should be temperature and humidity dependence on isotopic fractionation due to diffusion. Hence, in the relatively small natural temperature range we consider a as a linear function (to a first approximation) of absolute temperature (T) and vapour pressure (e) with parameter r_1 assigned to properties independent of meteorological parameters.

$$a = a_1T + a_2e + r_1. \quad (5)$$

(ii) Carboxylation and deposition being biochemical processes are temperature-dependent[34]. So b^* is considered a linear function (to a first approximation) of T. Properties independent of meteorological parameters are represented by r_2.

$$b^* = b_1T + r_2. \quad (6)$$

There are other factors known to effect cellulose formation in trees such as light intensity, metal ion concentration, etc. But, no long-term data of these is available for calibration in this reconstruction. Hence, these effects should be considered to be included in the parameters r_1 and r_2.

Substituting eqs (4)–(6) into eq. (3) we get

$$d = a_1T + a_2e + r_1 + (b_1 - a_1)\gamma\, Tz - a_2\gamma ez + (r_2 - r_1)\gamma z. \quad (7)$$

Estimation of model coefficients and error

Assuming $Tz = x$, $ez = y$, $(b_1 - a_1)\gamma = Q$, $a_2\gamma = -R$, $(r_2 - r_1)\gamma = S$ in eq. (7), we get an equation consisting of six variables. This equation is nonlinear, but is linearized by substitution of nonlinear combined variables.

$$d = a_1T + a_2e + r_1 + Qx + Ry + Sz. \quad (8)$$

For an accurate estimation of the coefficients of the above equation, we use inverse modelling for the overdetermined system in a box of size n (>6) for all time series variables, d, T, e and z (ref. 35).

$$D = MX \Rightarrow M^TD = M^TMX \Rightarrow X = \frac{M^TD}{M^TM}, \quad (9)$$

where $D = [d_i]$ is the column matrix of the d values of a certain tree, $M = [T_i\ e_i\ 1\ x_i\ y_i\ z_i] = 6 \times n$ matrix given by known variables, where $i = 1$ to n is the number of rows representing years, and $X = [a_1\ a_2\ r_1\ Q\ R\ S]^T$ is the column matrix of unknown constants to be evaluated.

Let N_j be the number of years a particular station j has data within the calibration period 1978–2005 CE. Hence upon estimation of the coefficients in the sliding box of size n, we get $(N_j - n)$ sets of coefficients. These sets of coefficients are then compared for internal variance. To have a significant comparison in this case and the minimum possible error in the coefficient estimation, we ran many trials to decide on $n = 10$ for all the stations. The calibration was thus achieved by sliding this 10-year

window through the period of data availability (N_j, which varied from a minimum of 16 to a maximum of 27). Matrix X was estimated using Moore–Penrose pseudo-inverse of matrices[35] and the software GNU Octave for $(N_j - n)$ groups of data. All runs were made with annual averages of T and e. d was calculated using the annual fitted $\delta^{13}C_a$.

Also from eq. (7), we get

$$z = \frac{d - (r_1 + a_1 T + a_2 e)}{[(b_1 - a_1)T - a_2 e + (r_2 - r_1)]\gamma} \tag{10}$$

$$= \frac{K}{L}, \text{ say;}$$

then from eq. (4)

$$c_a = sl - 100 * \ln\left(\frac{1}{z} - 1\right). \tag{11}$$

Equations (7) and (10) are respectively, the forward and inverse sides of the model. For $(N_j - n)$ sets of matrix X found from eq. (8), z was estimated ($\hat{z}$) using eq. (10) and the X giving minimum error in z (i.e. $\sqrt{\sum(z - \hat{z})^2}$) was selected for reconstructing $\hat{z}$ in the total period (1901–2005 CE) using eq. (10). These z-values are converted to c_a using eq. (11). Subsequently, the reconstructed c_a is compared with the observed c_a values in the testing period (1958–1977 CE).

Using error analysis theorems[36] on eq. (10) and considering $\delta^{13}C_a$, $\delta^{13}C_c$, T and e as mutually dependent, we get

$$\sigma_K^2 = \sigma_{\delta^{13}C_a}^2 + \sigma_{\delta^{13}C_c}^2 + a_1^2\sigma_T^2 + a_2^2\sigma_e^2$$

$$+ 2\sigma_{\delta^{13}C_a,\delta^{13}C_c}^2 + 2a_1\sigma_{\delta^{13}C_a,T}^2 + 2a_2\sigma_{e,\delta^{13}C_a}^2$$

$$+ 2a_1\sigma_{\delta^{13}C_c,T}^2 + 2a_2\sigma_{e,\delta^{13}C_c}^2 + 2a_1 a_2\sigma_{T,e}^2,$$

$$\sigma_L^2 = \gamma^2[(b_1 - a_1)^2\sigma_T^2 + a_2^2\sigma_e^2 - 2(b_1 - a_1)a_2\sigma_{T,e}^2],$$

$$\frac{\sigma_z^2}{z^2} = \frac{\sigma_K^2}{K^2} + \frac{\sigma_L^2}{L^2} - 2\frac{\sigma_{KL}^2}{KL}. \tag{12}$$

Also, from eq. (11):

$$\sigma_{c_a}^2 = \frac{100\sigma_z^2}{z(1-z)}, \tag{13}$$

where σ_i^2 and $\sigma_{i,j}^2$ respectively, represent the variance of parameter i and the covariance of parameters i and j.

The reconstruction model error (eq. (13)) is assigned at every time step for all the reconstructed c_a values. It is to be noted here that the error calculated in eq. (13) is the mathematical error which includes all the variabilities of the input parameters.

In this context it may be mentioned that we have considered globally averaged value of $\delta^{13}C_a$ for the following reason. $\delta^{13}C_a$ does show significant variability on seasonal timescale, especially in the high latitudes, but the annually averaged value has low variability. Hence we tried to quantify this effect by estimating the error on reconstructed c_a by taking the maximum variance of $\delta^{13}C_a$ as 1‰. This did not change the C_a variance significantly (<0.5 ppm).

On the other hand, the instrumental error in observed T and e is very small (which we cannot expect prior to 1901). We have tried to generalize the error analysis by taking standard deviation of data as error and not the given error (from CRU). But, the gridded data had low standard deviation or covariance with each other or the isotope data, which led to the □1.5 ppm model error (Table 1). Hence, unless any of the input datasets has a high standard deviation or covariance, we are likely to get similar levels of error.

Testing of the modified model

We have used two parameters to judge the reconstructed c_a: (i) P_r, the average absolute difference between observed global annual average c_a and model output c_a during the testing period (1957–1976) and (ii) $mxr\sigma$, the maximum reconstruction error among all time steps. The modified model (eqs (7) and (10)) was tested for sensitivity to input $\delta^{13}C_c$ data. For example, Figure 4 describes this for four different treatments of $\delta^{13}C_c$ for the site KOHP (chosen because it is the longer of the time series

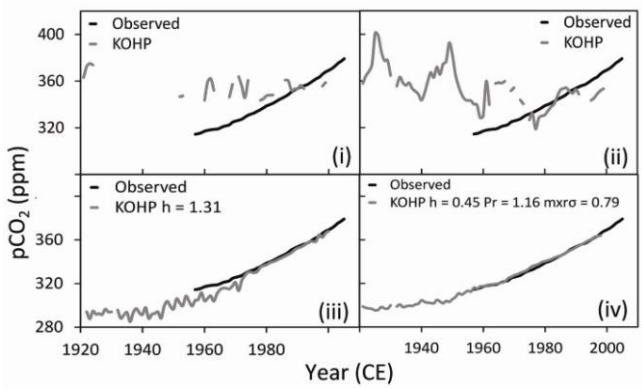

Figure 4. Time series of atmospheric c_a reconstructed from *P. smithiana* from Kothi, India (KOHP – grey lines) using our model, for four cases of pre-processing of $\delta^{13}C_c$: (i) Raw data; (ii) Smoothed by 30 years spline; (iii) Corrected using a fitted correction factor ($c_f = \delta^{13}C_a + hc_a$) with $d = -6.4$‰ $\delta^{13}C_c$; (iv) A combination of (ii) and (iii). The instrumentally observed c_a is shown by black line.

generated in this work). For comparison, we have also included in this figure the global annual average of observed c_a (2008–1957 CE). The same plot for the site LOSW is given in the Supplementary Information (Figure S1; see online). The following cases were tested:

(i) No treatment done on $\delta^{13}C_c$: the reconstructed c_a data do not show a good fit for the calibration period. The gaps in the reconstruction are due to the 5 ppm model error cap.

(ii) The data have been corrected for variability in tree growth pattern (e.g. juvenile/canopy effects) with a spline function at various levels[22]. Again, such input did not yield a better match with the observations.

(iii) Atmospheric pCO_2 rise due to anthropogenic activities affects plant $\delta^{13}C_c$ in two ways: (a) burning of fossil fuels depleted in ^{13}C leads to plants receiving pCO_2 with lowered $\delta^{13}C_a$ values; (b) The increase in c_a causes further discrimination against the heavier isotope (may be due to the change in pH of leaf water). Feng and Epstein[37] suggested a correction factor ($c_f = \delta^{13}C_a + hc_a$) to be applied to the $\delta^{13}C_c$ to compensate for these effects, where, h (‰/ppm) is the decrease in $\delta^{13}C_c$ due to (anthropogenic) increase in c_a. This correction factor (c_f) is calculated for the calibration years (with annual average c_a and $\delta^{13}C_a$) assuming h values (varied) and a quadratic fit was made as a function of years to extend it to 1901. This fitted value was used to correct $\delta^{13}C_c$ values for the years 1901–2005 CE (ref. 14). As $\delta^{13}C_a$ is already used in the correction, pre-industrial value of $\delta^{13}C_a = -6.4$‰ is used for this case for calculating d. The h value was varied from 0 to 1.4 with increment 0.001 to compensate for high P_r from earlier levels of h used (<0.05)[14,37]. h value used in the final reconstruction was determined by minimizing P_r. It is emphasized here that use of the observed c_a was limited to the calibration period alone and for the reconstruction and testing periods we have not used any observed c_a values.

(iv) $\delta^{13}C_c$ was spline corrected to 30 years to remove the effect of tree growth and then subjected to case (iii) correction. This yielded a smoother c_a, which in turn resulted in the least value of P_r.

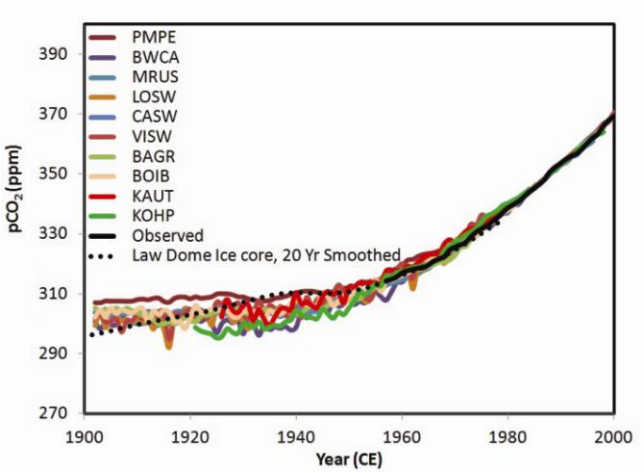

Figure 5. Reconstructed pCO_2 data for all stations compared with the instrumentally observed data (solid black) and ice-core data from Law Dome (dotted black).

From each site $\delta^{13}C_c$ data we reconstructed c_a and these data (Figure 5) with associated uncertainties are given in http://doi.pangaea.de/10.1594/PANGAEA.800072. The reconstructed data show that despite disparate trends observed in the original tree $\delta^{13}C_c$ datasets, our method way of accounting for the temperature and vapour pressure effects at each site results in mutually concordant c_a values.

Uncertainty estimation

Further, sensitivity analysis was done by varying h value from 0.001 to 1.4 in increment of 0.001 and studying the resultant pattern of P_r and $mxr\sigma$. For all stations, the h versus P_r plots (Figure 6) show that P_r decreases exponentially with increasing h, but characterized with some intermittent variations. The $h - mxr\sigma$ plot, in contrast is more irregular and $mxr\sigma$ approaches zero for high h, but ends with a few spikes. Since we cannot expect error values to vary widely from near zero to very high values due to small perturbations in h, such values of h have been avoided. Instead, the value of h that yields both P_r and $mxr\sigma$ lower than 1.5 ppm and close to each other is selected for reconstruction (Table 1). This makes P_r and $mxr\sigma$ equivalent in magnitude.

Figure 7 shows the sensitivity on reconstructed pCO_2 for different values of h for the site KOHP. Lower values (0.2 and 0.25) of h (light grey) show very high variability in the testing period (1958–1977). This leads to high values of P_r, as seen in the Figure 6 for the same site. If we decrease h further, then P_r will increase exponentially (Figure 6). But the change in variability is minimal in the range $h = 0.3$ to 0.65 (dark grey) and an optimum value is obtained at $h = 0.45$ (marked with filled dots). This shows that in this range the model is not sensitive to the variation in h and we can use any of these values without losing much accuracy of reconstruction.

We varied the saturation levels (sl) between 200 and 1000 ppm and calibrated for the minimum error in $z(\sqrt{\Sigma(z-\hat{z})^2})$. Among all samples, only PMPE gave resulting saturation level of 306 ppm. The rest showed a inverse relationship between sl and the error. This might be due to: (i) the effect of temperature rise on conductance in the leaf[38]; (ii) the sites showing inverse relationship are all conifers and the saturation behaviour in conifers is different than what is assumed here; this can be confirmed by inputing $\delta^{13}C$ data from more non-conifers in the future.

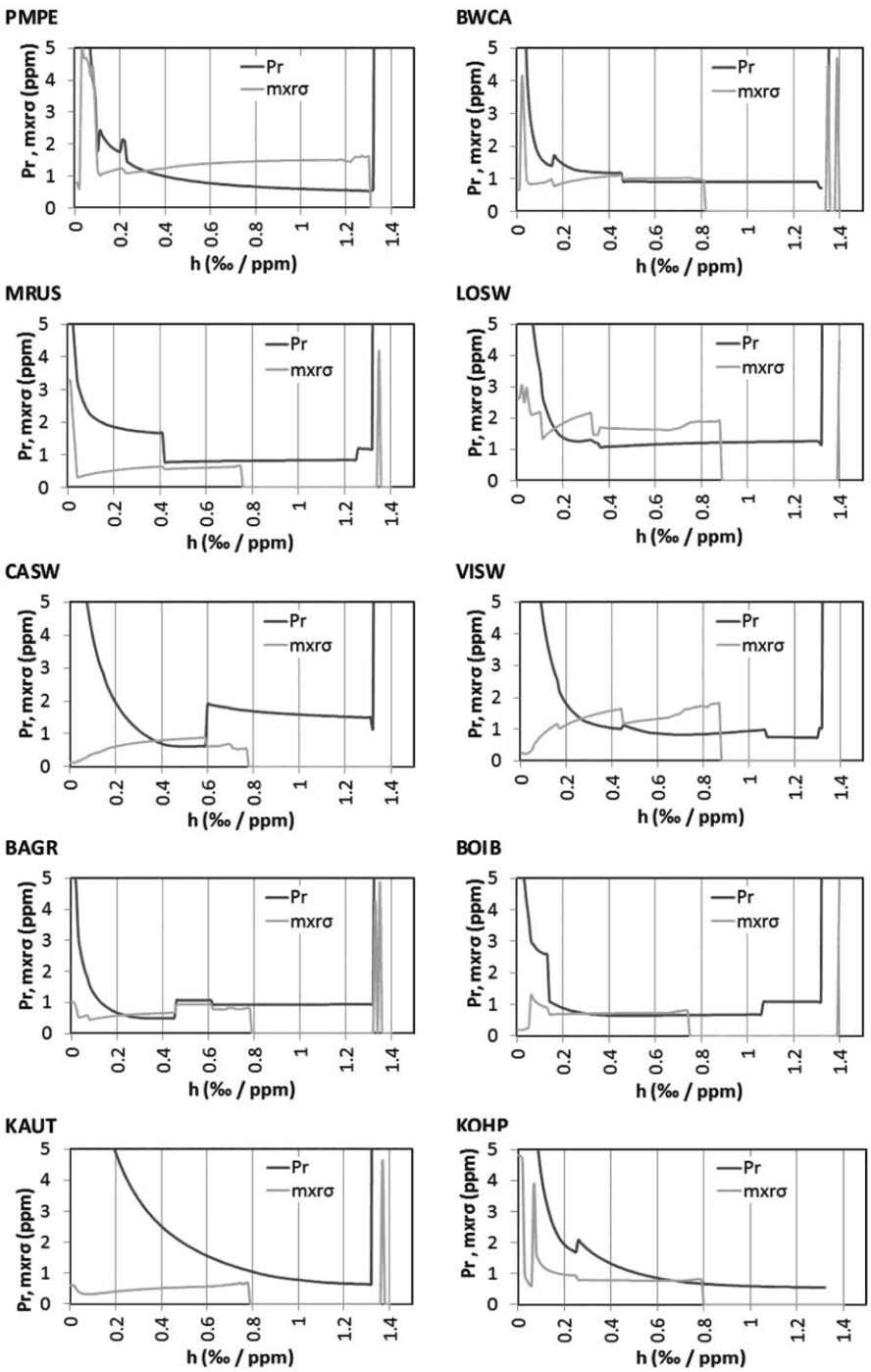

Figure 6. P_r (average absolute difference between observed global annual average c_a and model output c_a) and $mxr\sigma$ (maximum reconstruction error among all time steps) values with respect to variation in h for all stations. P_r decreases exponentially with increasing h, with some intermittent variations. The $h - mxr\sigma$ plot is irregular and for high h, $mxr\sigma$ approaches zero with a few spikes.

In all analyses, the maximum allowed estimation error was 5 ppm and the breaks seen in Figure 4(i) and (ii) are due to higher analytical errors at those points. It is to be noted that as the maximum error in reconstruction, i.e. P_r or $mxr\sigma$ is ~1.5 ppm, the reconstructions are to be considered accurate within this uncertainty (Table 1).

Comparison with other datasets

To test the reliability of the reconstructions, c_a data were compared with those from instrumental and ice-core datasets. The maximum spatial standard deviation of reconstructed c_a averaged globally at any time step yields

~5 ppm, which is comparable to ~4 ppm values for the observed data. The difference between global annual average observed c_a and reconstructed c_a at any site has a mean ~0.31 and standard deviation ~1.37 ppm with skewness ~0.21, showing that reconstruction errors are primarily random.

Assumption of a smooth global curve for $\delta^{13}C_a$ may be the cause of the wiggles in the reconstructed c_a, as variations in the observed $\delta^{13}C_a$ are not as smooth as those of observed c_a. This is the reason P_r cannot be decreased below a threshold. Many of the wiggles are coherent, which indicates that the value of $\delta^{13}C_a$ assumed in that period may not be strictly valid. This can possibly provide corrections for the $\delta^{13}C_a$ curve by backtracking, as this information is unavailable in high-resolution ice-core data.

The applicability of our model may be verified by comparing the observed pCO_2 gradient (between the tropics and the mid latitudes) with that of the model-derived data. As only one of the sites (PMPE) is in the tropics, we depict this gradient by plotting its values with respect to the reconstructed value for the site BWCA (Figure 8). For comparison with observations, we selected two datasets in comparable latitudes: (a) Cape Fergusson, Australia (CSIRO) and (b) La Jolla Pier, California, USA (SIO). The two grey points represent the mean value for the months of June during 1992–2006 for these sites. The mean (1902–1957) of the reconstructed data is given in black colour. This plot compares that the latitudinal gradient in observed (slope: –0.146 ppm/°; intercept: 362.977 ppm) and reconstructed data (slope: –0.150 ppm/°; intercept: 307.830 ppm). A good agreement between the observed and reconstructed slope gives credence to our model.

Comparison with the ice-core data from Law Dome (Figure 9) shows that the difference (D) between pCO_2 derived from ice core and all tree-ring sites remains mostly 0 ± 4 ppm till 1960s; prior to this it rises until 1931–1940 CE with different amplitudes for different sites. This amplitude of D correlates well with latitude (r = 0.55, P < 0.10), implying its dependence on the distance from Antarctica. Also, the adjacent sites show similar amplitude values. The maximum D observed was ~12.5 ppm at BWCA. Before 1931, it decreases gradually to reach a near-zero level around 1910. In some sites it goes below –5 ppm at ~1908 (e.g. PMPE site). We rule out the possibility of any model bias being responsible for the D values because: (a) the difference is not seen throughout the reconstruction period; (b) the timing of maximum difference does not coincide among sites, and (c) the magnitudes of the differences are not identical. Possible reasons for this discrepancy are discussed later.

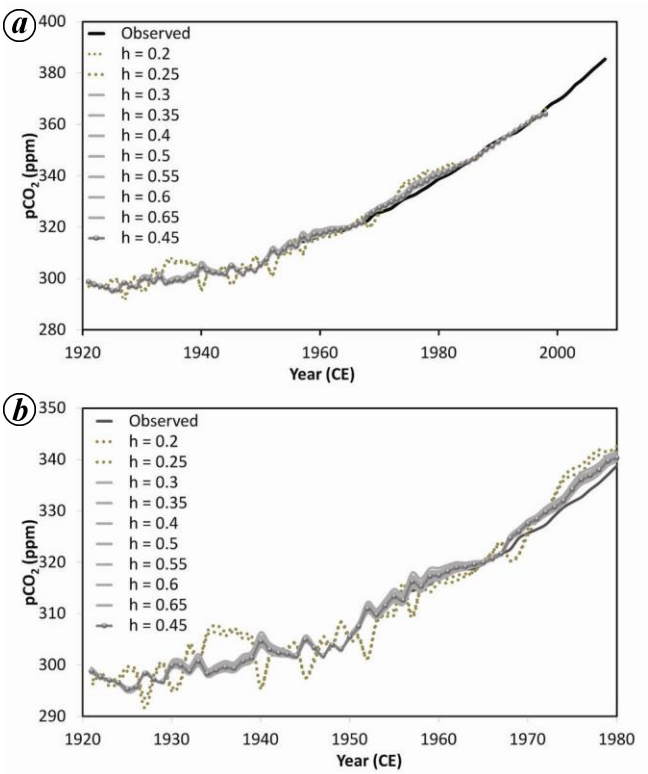

Figure 7. Sensitivity of the model is tested against h (‰/ppm) for the $\delta^{13}C_c$ from Kothi, India (KOHP). ***a***, The whole period (1920–2000). ***b***, The reconstruction period, including testing period (1920–1978). The lightest shades are used for the lowest values of h (0.2 and 0.25) as they cause the most deviation. The rest show small, random spreads around the best estimation of c_a for h = 0.45 (shadow circled).

Discussion and conclusion

Testing of various processing schemes of $\delta^{13}C_c$ data reveals that the model is sensitive to the processing of input

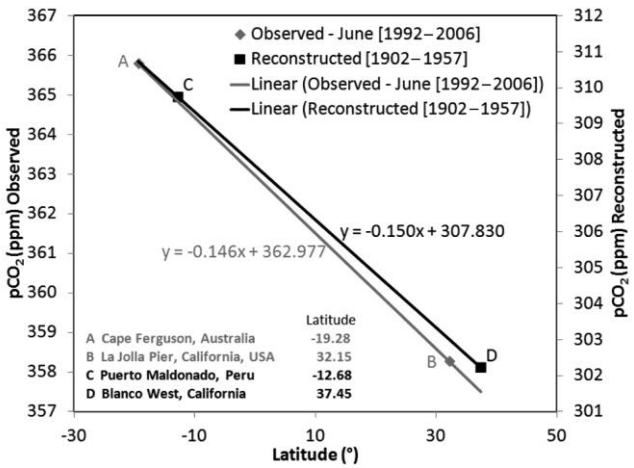

Figure 8. Comparison of model-derived pCO_2 against observed June pCO_2 values showing latitudinal gradient between tropics and mid-latitudes. Two sites each have been chosen from the southern tropics and northern mid-latitudes (as these have the highest gradient) based on availability. The observed data (mean of 1992–2006 June months) are taken from CSIRO and SIO pCO_2 databases respectively, and are shown in grey. The model-derived data (mean of 1902–1957) are shown in black.

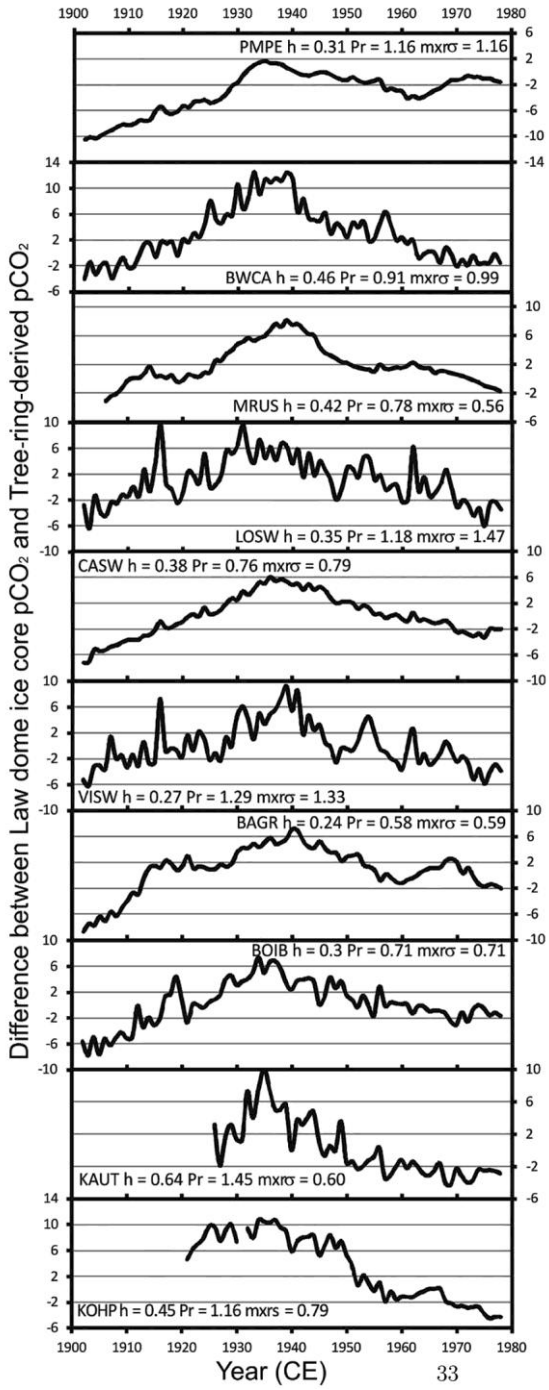

Figure 9. Each panel displays the difference between the Law Dome c_a records and the tree-ring-based c_a variation for a given site during 1978–1901 CE. The *y*-axis represents the difference between the Law Dome c_a records and the tree-ring-based c_a (uncertainty = maximum of P_r and $mxr\sigma$) for that site (in ppm). *h* is the coefficient of c_a in the model (eq. (14)), P_r the average absolute difference among observed global annual average c_a and model output c_a during the testing period (1957–1976 CE) and $mxr\sigma$ is the maximum reconstruction error between all time steps. Each site shows very small difference between these two datasets during 1978–1960 CE. Prior to this, broad maxima are observed with peaks in ~1931–1940 CE, which implies a higher c_a value at Antarctica compared to the tropics and the northern hemisphere. The difference reduces to zero again around 1910 CE. The maximum difference is significantly correlated with latitude, showing a dependence on the distance from the Antarctic site.

$\delta^{13}C_c$. This implies that the value of *d* in natural samples not only depends on the ratio c_i/c_a, but also on the absolute values of c_a. Hence, hc_a should be considered an inherent part of the model and not a mere correction applied to remove anthropogenic effect on c_a. So, the final form of *d* turns out to be

$$\begin{aligned} d + 6.4 - hc_a &= a + (b-a)\frac{c_i}{c_a} \\ &= a_1 T + a_2 e + r_1 + (b_1 - a_1)\gamma T z \\ &\quad - a_2 \gamma e z + (r_2 - r_1)\gamma z. \end{aligned} \tag{14}$$

Notably, Feng and Epstein[37] proposed the correction for c_a as the correction for the higher c_a values in the latter part of the 20th century. Instead, our study shows the factor (hc_a) in eq. (14) needs to be applied for both higher (~380 ppm) and lower (~280 ppm) ranges of c_a spanning the entire last century (Figure 4). This means that the modified value is important in terms of tree chemistry and is observed only in the presence of a significant and persistent temporal trend in c_a. Although this high value of *h* appears to be a limitation of the model, it is justified by considering the fractionation factors (*a*, *b*) as not constant but temperature- and humidity-dependent; the last few decades experienced unprecedented rate in rise in both temperature and c_a, which must have affected the tree chemistry and as a result the carbon isotope fractionation. The earlier estimates for this constant involved trials to increase the linear correlation with the meteorological parameters[14,37] and nonlinear variabilities were not considered. Also, this correction does not have a linear effect on reconstruction as that is derived primarily from a nonlinear (exponential) function.

Table 1 shows that the *h* values of samples from the same genus are similar even when growing in contrasting climates, e.g. KOHP in India (*P. smithiana*) and MRUS in Siberia (*Picea obovata*). On the other hand, samples from different genera from nearby sites show quite different *h* values, e.g. CASW (*Quercus petraea*) and VISW (*Pinus sylvestris*). This implies that *h* value is primarily species-dependent.

Figure 9 shows that *D* is high during 1960–1910, with maximum in 1940–1931 at all the sites. Possible causes for this anomaly include:

(i) Decrease in industrial production in the northern hemisphere during this period, as the times of maxima coincide with the Great Depression and the beginning of the Second World War.
(ii) Increase in plant productivity due to the temperature maximum in the northern hemisphere[39].
(iii) Possible increased CO_2 supply from deep ocean near Law Dome area (as known in present times from Takahashi *et al.*[40]). But due to lack of contemporary data we cannot confirm this hypothesis.

Our model for reconstructing c_a from tree-ring cellulose has a few advantages over the c_a data conventionally retrieved from ice cores. First, ice sheets accumulate only in the polar regions during the present. Therefore, c_a values reconstructed from ice cores are mostly confined to polar regions. Second, ice-core records have limited overlap with the period of instrumental data (1958 and later), which limits their scope for validation. Third, their resolution decreases with time as snow compacts to fern and further to ice. Moreover, trapping of CO_2 in ice layers depends on snowfall rate that may have seasonality, causing bias in flux estimation. Lastly, ice-core dating requires substantial logistic support and manpower. The tree-ring-based reconstruction of c_a, on the other hand, overcomes many of these problems. Dating of tree rings is a straightforward process and can be achieved with minimal resources. Trees can be dated with annual resolution as far back as 11,000 years in time[41]. They extend geographically from the tropics to high latitudes. Our study presents, a reconstructed dataset which depicts the observed summer latitudinal gradient emphasizing the compatibility of the reconstruction with the observations. This study, therefore, expands the scope of carbon dynamics study spatially as well as temporally from the 1950s to about the early Holocene.

The present work is limited by the availability of temperature and vapour pressure data, i.e. to only till the beginning of the 20th century for most places. For earlier times, temperature reconstructions are available from various sources, including tree-ring-based ones from similar sites with annual resolutions[42,43]. Also available are the drought estimates from tree-ring sites with implied moisture levels[44,45]. Using these datasets in the presented model, it is possible to reconstruct c_a for the entire duration of available tree-ring chronologies, albeit with higher error levels (as the error in the present reconstruction includes the errors in temperature and vapour pressure inputs). However, as the error levels in our model are taken as the variance of the input data, this increase might not be very high as most temperature reconstructions do not have high standard deviation[46].

The proposed modifications to the carbon isotope model for tree rings add complications to the original model by inclusion of recently available data and information. Further parameterization, including various tree (e.g. metal ion concentration), soil (e.g. chemical contamination) or physical parameters (e.g. light intensity) can be added in future when long-term data of these become available for calibration in the annual to multidecadal scale for use in the palaeoclimatic studies. Even with limited amount of added complexities, the presented model reconstructs the c_a data for all latitudes, from tropical (PMPE) to boreal (MRUS) with reasonable coherence.

Most importantly, this study has the potential to reconstruct the seasonal pCO_2 variation across the latitudes facilitating carbon cycle study in high temporal resolution. Hence, this model can further be tuned from annual to seasonal resolution on the basis of tree-ring samples separated into early and late woods in the growing season[6]. In addition to estimation of past c_a in the tropics and subtropics, our model separates meteorologically dependent effects in carbon isotopic fractionation from the independent ones, i.e. effects of species, location, etc. Removal of meteorologically independent coefficients may facilitate studies of future tree–atmosphere interactions vis-à-vis climate.

1. Rödenbeck, C., Houweling, S., Gloor, M. and Heimann, M., CO_2 flux history 1982–2001 inferred from atmospheric data using a global inversion of atmospheric transport. *Atmos. Chem. Phys.*, 2003, **3**(6), 1919–1964.
2. Meure, C. M. *et al.*, Law dome CO_2, CH_4 and N_2O ice core records extended to 2000 years BP. *Geophys. Res. Lett.*, 2006, **33**(14).
3. Ahn, J. *et al.*, Atmospheric CO_2 over the last 1000 years: A high-resolution record from the West Antarctic Ice Sheet (WAIS) divide ice core. *Global Biogeochem. Cycles*, 2012, **26**(2).
4. Barnola, J. M., Anklin, M., Porcheron, J., Raynaud, D., Schwander, J. and Be Stauffer, CO_2 evolution during the last millennium as recorded by Antarctic and Greenland ice. *Tellus B*, 1995, **47**(1–2), 264–272.
5. Kheshgi, H. S., Prince, R. C. and Marland, G., The potential of biomass fuels in the context of global climate change: focus on transportation fuels 1. *Annu. Rev. Energy Environ.*, 2000, **25**(1), 199–244.
6. Schweingruber, F. H., *Tree Rings – Basics and Applications of Dendrochronology*, D. Reidel Publishing Company, 1988.
7. Leavitt, S. W. and Danzer, S. R., Method for batch processing small wood samples to holocellulose for stable-carbon isotope analysis. *Anal. Chem.*, 1993, **65**(1), 87–89.
8. Managave, S. R. and Ramesh, R., Isotope dendroclimatology: A review with a special emphasis on tropics. In *Handbook of Environmental Isotope Geochemistry* (ed. Baskaran, M.), Springer, 2012, pp. 811–833.
9. Robertson, I., Switsur, V. R., Carter, A. H. C., Barker, A. C., Waterhouse, J. S., Briffa, K. R. and Jones, P. D., Signal strength and climate relationships in $^{13}C/^{12}C$ ratios of tree ring cellulose from oak in East England. *J. Geophys. Res. D*, 1997, **102**(16), 19507–19519.
10. Arens, N. C., Hope Jahren, A. and Amundson, R., Can C_3 plants faithfully record the carbon isotopic composition of atmospheric carbon dioxide? *Paleobiology Winter*, 2009, **26**(1), 137–164.
11. Chakraborty, S., Dutta, K., Bhattacharyya, A., Nigam, N., Schuur, E. A. G. and Shah, S. K., Atmospheric ^{14}C variability recorded in tree rings from Peninsular India: implications for fossil fuel CO_2 emission and atmospheric transport. *Radiocarbon*, 2008, **50**(3), 321–330.
12. Holzkämper, S., Kuhry, P., Kultti, S., Gunnarson, B. and Sonninen, E., Stable isotopes in tree rings as proxies for winter precipitation changes in the Russian arctic over the past 150 years. *Geochronometria*, 2008, **32**(1), 37–46.
13. Saurer, M., Cherubini, P., Reynolds-Henne, C. E., Treydte, K. S., Anderson, W. T. and Siegwolf, R. T. W., An investigation of the common signal in tree ring stable isotope chronologies at temperate sites. *J. Geophys. Res. G*, 2008, **113**(4), G04035.
14. Treydte, K. S., Frank, D. C., Saurer, M., Helle, G., Schleser, G. H. and Esper, J., Impact of climate and CO_2 on a millennium-long tree-ring carbon isotope record. *Geochim. Cosmochim. Acta*, 2009, **73**(16), 4635–4647.
15. Kress, A., Saurer, M., Siegwolf, R. T. W., Frank, D. C., Esper, J. and Bugmann, H., A 350 year drought reconstruction from

alpine tree ring stable isotopes. *Global Biogeochem. Cycles*, 2010, **24**(2).
16. Ballantyne, A. P., Baker, P. A., Chambers, J. Q., Villalba, R. and Argollo, J., Regional differences in South American monsoon precipitation inferred from the growth and isotopic composition of tropical trees. *Earth Inter.*, 2011, **15**(5), 1–35.
17. Bale, R. J. *et al.*, An annually resolved bristlecone pine carbon isotope chronology for the last millennium. *Quaternary Res.*, 2011, **76**(1), 22–29.
18. Schubert, B. A. and Hope Jahren, A., Fertilization trajectory of the root crop Raphanus sativus across atmospheric pCO_2 estimates of the next 300 years. *Agric. Ecosyst. Environ.*, 2011, **140**(1), 174–181.
19. Schubert, B. A. and Hope Jahren, A., The effect of atmospheric CO_2 concentration on carbon isotope fractionation in C_3 land plants. *Geochim. Cosmochim. Acta*, 2012, **96**, 29–43.
20. Farquhar, G. D., O'Leary, M. H. and Berry, J. A., On the relationship between carbon isotope discrimination and the intercellular carbon dioxide concentration in leaves. *Austr. J. Plant Physiol.*, 1982, **9**(2), 121–137.
21. Evans, J. R. and Von Caemmerer, S., Carbon dioxide diffusion inside leaves. *Plant Physiol.*, 1996, **110**(2), 339.
22. McCarroll, D. *et al.*, Correction of tree ring stable carbon isotope chronologies for changes in the carbon dioxide content of the atmosphere. *Geochim. Cosmochim. Acta*, 2009, **73**(6), 1539–1547.
23. Borgaonkar, H. P., Ram, S. and Sikder, A. B., Assessment of tree-ring analysis of high-elevation Cedrus deodara D. Don from Western Himalaya (India) in relation to climate and glacier fluctuations. *Dendrochronologia*, 2009, **27**(1), 59–69.
24. Borgaonkar, H. P., Sikder, A. B. and Ram, S., High altitude forest sensitivity to the recent warming: a tree-ring analysis of conifers from Western Himalaya, India. *Quaternary Int.*, 2011, **236**(1), 158–166.
25. Helle, G. and Schleser, G. H., Beyond CO_2-fixation by Rubisco – an interpretation of $^{13}C/^{12}C$ variations in tree rings from novel intra-seasonal studies on broad-leaf trees. *Plant Cell Environ.*, 2004, **27**(3), 367–380.
26. Keeling, C. D., Piper, S. C., Bacastow, R. B., Wahlen, M., Whorf, T. P., Heimann, M. and Meijer, H. A., Atmospheric CO_2 and $^{13}CO_2$ exchange with the terrestrial biosphere and oceans from 1978 to 2000: observations and carbon cycle implications. In *A History of Atmospheric CO_2 and its Effects on Plants, Animals, and Ecosystems*, Springer, 2005, pp. 83–113.
27. Yakir, D., The stable isotopic composition of atmospheric CO_2. In *Treatise Geochemistry* (ed. Keeling, R. F.), Elsevier, 2003, vol. 4, pp. 175–212.
28. Levin, I., Graul, R. and Trivett, N., Long-term observations of atmospheric CO_2 and carbon isotopes at continental sites in Germany. *Tellus B*, 1995, **47**(1–2), 23–34.
29. Mitchell, T. D. and Jones, P. D., An improved method of constructing a database of monthly climate observations and associated high-resolution grids. *Int. J. Climatol.*, 2005, **25**(6), 693–712.
30. McCarroll, D. and Loader, N. J., Stable isotopes in tree rings. *Quaternary Sci. Rev.*, 2004, **23**(7), 771–801.
31. Doney, S. D., Fabry, V. J., Feely, R. A. and Kleypas, J. A., Ocean acidification: the other CO_2 problem. *Marine Sci.*, 2009, **1**.
32. Edwards, T. W. D., Graf, W., Trimborn, P., Stichler, W., Lipp, J. and Payer, H. D., $\delta^{13}C$ response surface resolves humidity and temperature signals in trees. *Geochim. Cosmochim. Acta*, 2000, **64**(2), 161–167.
33. Philibert, J., One and a half century of diffusion: Fick, Einstein, before and beyond. *Diffusion Fundam.*, 2006, **4**(6), 1–19.
34. Connors, K. A., *Chemical Kinetics: The Study of Reaction Rates in Solution*, Wiley-VCH, 1990.
35. Strang, G., *Introduction to Linear Algebra*, SIAM, 2003.
36. Bevington, P. R. and Keith Robinson, D., *Data Reduction and Error Analysis for the Physical Sciences, Volume 2*, McGraw-Hill, New York, 1969.
37. Feng, X. and Epstein, S., Carbon isotopes of trees from arid environments and implications for reconstructing atmospheric CO_2 concentration. *Geochim. Cosmochim. Acta*, 1995, **59**(12), 2599–2608.
38. Bernacchi, C. J., Portis, A. R., Nakano, H., von Caemmerer, S. and Long, S. P., Temperature response of mesophyll conductance. Implications for the determination of Rubisco enzyme kinetics and for limitations to photosynthesis *in vivo*. *Plant Physiol.*, 2002, **130**(4), 1992–1998.
39. Solomon, S. D. *et al.* (eds), *Climate Change 2007: The Physical Science Basis. Contribution of Working Group I to the Fourth Assessment Report of the Intergovernmental Panel on Climate Change*, Cambridge University Press, Cambridge, United Kingdom, 2007.
40. Takahashi, T., Feely, R. A., Weiss, R. F., Wanninkhof, R. H., Chipman, D. W., Sutherland, S. C. and Takahashi, T. T., Global air–sea flux of CO_2: an estimate based on measurements of sea–air pCO_2 difference. *Proc. Natl. Acad. Sci. USA*, 1997, **94**(16), 8292–8299.
41. McGovern, P. E. *et al.*, Science in archaeology: a review. *Am. J. Archaeol.*, 1995, **99**(1), 79–142.
42. Briffa, K. R., Jones, P. D. and Schweingruber, F. H., Tree-ring density reconstructions of summer temperature patterns across western North America since 1600. *J. Climate*, 1992, **5**, 735–754.
43. Esper, J., Cook, E. R. and Schweingruber, F. H., Low-frequency signals in long tree-ring chronologies for reconstructing past temperature variability. *Science*, 2002, **295**(5563), 2250–2253.
44. Herweijer, C., Seager, S., Cook, E. R. and Emile-Geay, J., North American droughts of the last millennium from a gridded network of tree-ring data. *J. Climate*, 2007, **20**(7), 1353–1376.
45. Leavitt, S. W., Chase, T. N., Rajagopalan, B., Lee, E., Lawrence, P. J. and Woodhouse, C. A., Southwestern US drought maps from pinyon tree-ring carbon isotopes. *EOS, Trans. Am. Geophys. Union*, 2007, **88**(4), 39–40.
46. Ljungqvist, F. C., A new reconstruction of temperature variability in the extra-tropical northern hemisphere during the last two millennia. *Geogr. Ann.: Ser. A, Phys. Geogr.*, 2010, **92**(3), 339–351.

ACKNOWLEDGEMENTS. We thank M. Saurer (PSI, Switzerland) for providing data and all those who have contributed their data to the NOAA palaeoclimate database. We are grateful to V. K. Gaur (C-MMACS, Bangalore), for active support in formulating and coding of the model; Y. K. Tiwari for providing valuable input to atmospheric pCO_2 data interpretation; S. Mahapatra, S. Saha, C. Gnanaseelan, N. Singh, N. R. Deshapande, M. V. S. Ramarao and S. Haldar for help in various stages of analysis, and Prof. B. N. Goswami (Director, Indian Institute of Tropical Meteorology, Pune) for encouragement. IITM is fully funded by the Ministry of Earth Science, New Delhi. Tree-ring samples from Western Himalayas were collected under ISRO–GBP–Dendro project.

Received 25 April 2014; revised accepted 27 June 2014